# Self-assembly of a short amphiphile in water controlled by superchaotropic polyoxometalates: H4SiW12O40 vs. H3PW12O40

Philipp Schmid, Thomas Buchecker, Ali Khoshsima, Didier Touraud, Olivier Diat, Werner Kunz, Arno Pfitzner, Pierre Bauduin

Contents lists available at ScienceDirect

Journal of Colloid and Interface Science

journal homepage: www.elsevier.com/locate/jcis

# Self-assembly of a short amphiphile in water controlled by superchaotropic Polyoxometalates: $H_4SiW_{12}O_{40}$ vs. $H_3PW_{12}O_{40}$

Philipp Schmid [a, b], Thomas Buchecker [a, b], Ali Khoshsima [c, d], Didier Touraud [d], Olivier Diat [b], Werner Kunz [d], Arno Pfitzner [a], Pierre Bauduin [b, *]

[a] *Institute of Inorganic Chemistry, University of Regensburg, 93040 Regensburg, Germany*
[b] *Institut de Chimie Séparative de Marcoule, ICSM, CEA, CNRS, ENSCM, Univ Montpellier, Marcoule, France*
[c] *School of Petroleum and Petroleum and Chemical Engineering, Hakim Sabzevari University, Sabzevar, Iran*
[d] *Institute of Physical and Theoretical Chemistry, University of Regensburg, 93040 Regensburg, Germany*

## GRAPHICAL ABSTRACT

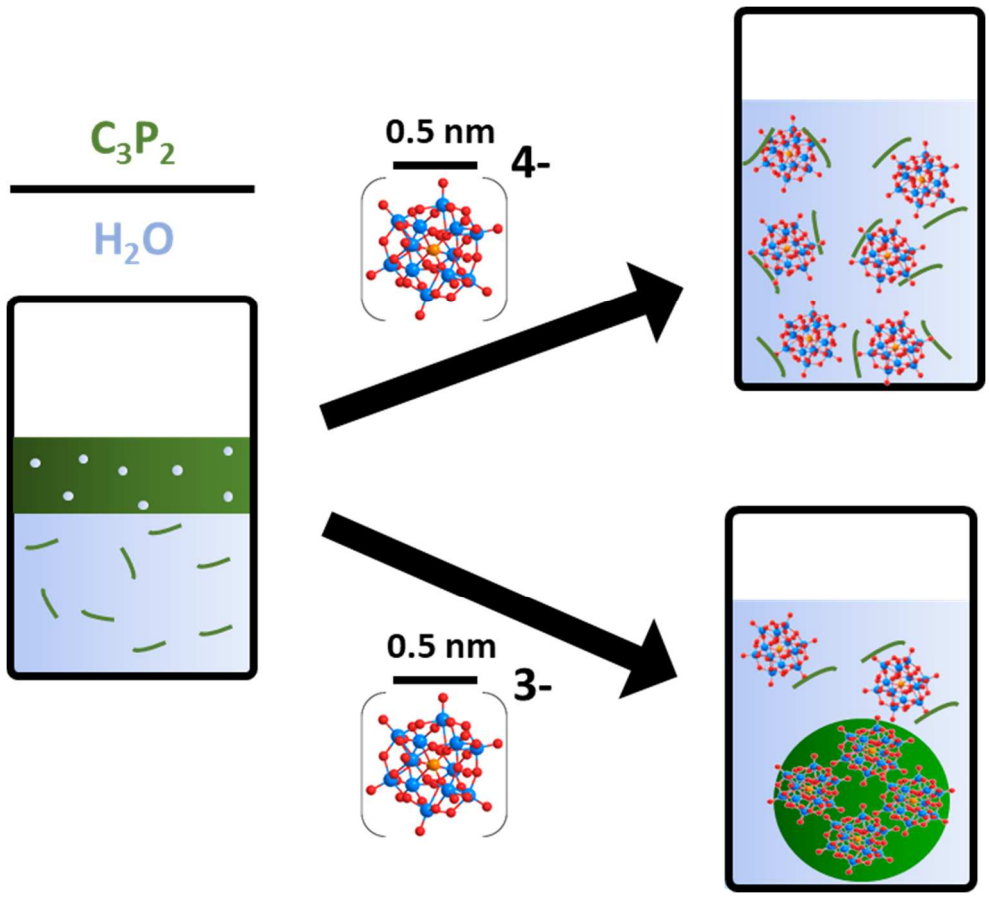


Keywords: Superchaotropicity · Polyoxometalates · mesoscopic structuring · Colloids · Adsorption · Self-assembly

## ABSTRACT

Nanometric ions, such as polyoxometalates (POMs) or ionic boron clusters, with low charge density have previously shown a strong propensity to bind to macrocycles and to adsorb to neutral surfaces: micellar, surfactant covered water-air and polymer surfaces. These association phenomena were shown to arise from a solvent-mediated effect called the (super-)chaotropic effect. We show here by combining cloud point (CP) measurements, scattering (SAXS/SANS) and spectroscopic techniques (NMR) that Keggin`s POMs: $H_4SiW_{12}O_{40}$ (SiW) and $H_3PW_{12}O_{40}$ (PW), induce the self-assembly of an organic solvent: dipropylene glycol n-propylether ($C_3P_2$), in water. The strong interaction between SiW/PW with $C_3P_2$ leads to a drastic increase in the CP, and aqueous solubility, of $C_3P_2$, *e.g.* SiW enables reaching full water-$C_3P_2$ co-miscibility at room temperature. At high POM concentrations, SiW leads to a continuous increase of the CP, forming $[SiW][C_3P_2]_{1\text{-}2}$ complexes, whereas PW produces a decrease in the CP attributed to the formation of nearly "dry" spherical $[PW]_n[C_3P_2]_m$ colloids, with n~4 and m~30. At high $C_3P_2$/PW contents, the $[PW]_n[C_3P_2]_m$ colloids turn into large interconnected structures, delimiting two pseudo-phases: a PW-$C_3P_2$-rich phase and a water-rich phase. It is proposed that the stronger electrostatic repulsions between SiW (4-), compared to PW (3-), prevents the formation of mesoscopic colloids.


## 1. Introduction

Only recently, nanometric ions, called nano-ions (NIs), have been shown to strongly (*i*) adsorb to surfaces covered with hydrated moieties, *e.g.* sugars, polyethylene glycols at micellar or water-air surfaces, [1][2][3] and (*ii*) to bind to the cavity of macrocycles, *e.g.* cyclodextrins[4][5]. The unexpectedly strong binding of NIs with these electrically neutral systems was described as a "superchaotropic" behavior [1][4][6] by comparison with the effect of classical (smaller) chaotropic ions such as iodide ($I^-$) or thiocyanate ($SCN^-$), usually classified in the Hofmeister series.[7][8] It was proposed that the superchaotropic effect, or superchaotropicity (SC), is a solvent- (water-) mediated phenomenon, emerging from the favorable release of (high energy) water molecules from the hydrated surface moieties (or the interior of macrocycles) and from the weakly hydrated NIs towards bulk water upon adsorption/binding.[1] The strength of the SC effect of different polyoxometalates (POMs), was evaluated by their influence on the clouding temperature of a non-ionic surfactant, tetraethylene glycol monooctylether ($C_8E_4$), and by the strength of their adsorption on $C_8E_4$ micelles which were characterized by an adsorption constant in the millimolar range.[2] From the classification of different POMs obtained with this approach, it was concluded that the overall charge density of the NIs is a decisive parameter in their SC behavior, *i.e.* the lower the charge density, the stronger the SC behavior, the stronger the binding. Remarkably, the SC effect appeared to be independent of the chemical nature of the nano-ions. Indeed, a wide variety of nano-ions, such as boron clusters[4][6] and hydrophobic ions, *e.g.* tetraphenyl-borate or -phosphonium[9][10], were classified as superchaotropes. In a recent work, all these nano-ions were investigated and unified regarding their effect on the phase behavior of non-ionic polyethoxylated surfactants ($C_iE_j$).[11] It was concluded that NIs, independently of their chemical nature, act similarly to ionic surfactants when mixed with polyethoxylated surfactants, *i.e.* both NIs and ionic surfactants bring charges to the non-ionic surfactant aggregates (micelles or lyotropic phase). The mechanism of NIs differs from the one of (anionic) surfactants, as NIs stick at the surface of non-ionic aggregates by a dehydration process, *i.e.* upon the SC effect, whereas for anionic surfactants their alkyl chains are anchored in the non-ionic aggregates by the hydrophobic effect. However NIs, with some exceptions such as the boron clusters from the metalla bis-dicarbollide class,[12] are not surfactants by themselves as they are not surface-active, neither form micelle or lyotropic phases in water. It is worth mentioning here that an official definition of SC, and clear distinction between SC and hydrophobicity, is still missing and that this point is still actively under debate in the community.[13] In the recent years, the binding of POMs was observed on hydrophilic neutral solutes, namely (oligomeric) polyethylene glycol (PEG)[3] and poly-N-isopropylacrylamide (PNiPAM)[14]. Both systems are linear chains, non-amphiphilic and they do not self-assemble at low concentrations when they are in water. Nevertheless, POMs of the α-Keggin type,

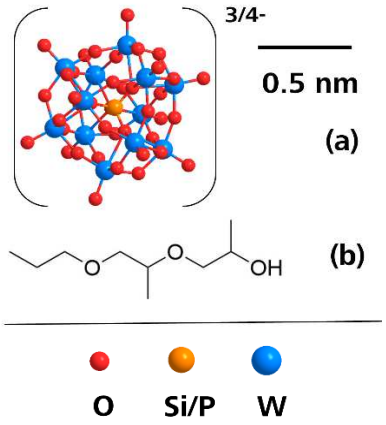


**Fig. 1.** (a) Representative structure of α-Keggin-type polyoxometalate anion (*i.e.* $PW_{12}O_{40}^{3-}$ (PW), $SiW_{12}O_{40}^{4-}$ (SiW)) and (b) an isomer of $C_3P_2$. Note, that in the present study only the acidic forms of the POMs, *i.e.* $H_3PW_{12}O_{40}$ and $H_4SiW_{12}O_{40}$, are considered.

namely the phosphotungstate, $PW_{12}O_{40}^{3-}$ (PW), and silicotungstate, $SiW_{12}O_{40}^{4-}$ (SiW), see Fig. 1a, were found to interact strongly, through the SC effect, with PEG and PNiPAM to form nano-assemblies: PEG-decorated POMs and large sheet/globular structures respectively.[3][14] There exclusively the acidic POM forms were used which is noteworthy, as POMs already provide different behaviors in water by exchanging the POM`s cation.[15] As a conclusion, the binding (or SC behavior) of NIs with these latter hydrophilic polymeric solutes induces their self-assembly in a wide variety (size and shape) of supramolecular structures. It was also shown that the binding of POMs with neutral macrocycles enabled to elaborate complex hybrid materials with nanometric structuration.[16] In the present contribution, we investigate further the interaction between NIs and organic neutral solutes, by focusing on PW and SiW in water with an organic solvent, which is a short chain amphiphilic molecule, the di-propylene glycol n-propylether ($C_3P_2$), see Fig. 1b. $C_3P_2$ is an industrial organic solvent used in diverse applications fields, such as in cleaners, cosmetics and coatings/paints.[17] It belongs to a class of molecules known as “hydrotrope”, which refers to short amphiphilic molecules.[18][19][20] The alkyl chain of a hydrotrope (its hydrophobic part) is too short (or too small) to induce micellization at relatively low concentrations (< 0.1 mol $L^{-1}$), as it is observed with true surfactants having a linear alkyl chain with at least seven carbon atoms.[21] Compared to surfactants, forming well-defined micelles at low concentrations (< 0.1 mol $L^{-1}$), most of the hydrotropes form ill-defined “aggregates” at high concentrations in water typically above 0.5 mol $L^{-1}$.[18][22]

Hence, $C_3P_2$ is, compared to the previously investigated solutes, *i.e.* non-ionic polymers (PEG, PNiPAM), macrocycles and surfactants ($C_iE_j$)[2][3][4][14], an interesting candidate to investigate the SC effect of POMs as:

*(i)* it has a low molecular weight and shows a more pronounced hydrophobic character, leading to a partial co-miscibility with water at room temperature

*(ii)* it enables to work on both, the monomeric state (non-aggregated) at low $C_3P_2$ concentrations and on ill-defined aggregates (typical for hydrotropes) at high concentrations.

Moreover, $C_3P_2$ is well known to be thermosensitve as it shows a cloud point (CP) in water with a lower critical solubilization temperature (LCST) at ~14 °C [23][24]. The evolution of the CP of $C_3P_2$ by adding different salts was previously proposed as a convenient and representative method to investigate the kosmotrope/chaotrope behavior of salts and therefore specific salt effects.[25] Consequently, the evolution of the CP of $C_3P_2$ by the addition of POMs is investigated here to monitor the SC effect. The results are compared to similar CP experiments previously performed on other thermosensitive systems: $C_8E_4$ surfactant[1][2] and PNiPAM.[14] The formation of supramolecular structures, *i.e.* POM-$C_3P_2$ assemblies in water, in the PW(/SiW)/$C_3P_2$ aqueous systems is investigated by combining small angle X-ray and neutron scattering (SAXS and SANS) and $^1$H-nuclear magnetic resonance ($^1$H-NMR).

## 2. Materials and methods

### *2.1 Materials*

Phosphotungstic acid hydrate ($H_3PW_{12}O_{40} \cdot x\ H_2O$, PW, MW = 2898 g/mol, 99.995% purity), silicotungstic acid hydrate ($H_4SiW_{12}O_{40} \cdot x\ H_2O$, SiW, MW = 2878 g/mol), phosphomolybdic acid hydrate ($H_3PMo_{12}O_{40} \cdot x\ H_2O$, PMo, MW = 1825 g/mol) and NaSCN were purchased from Sigma Aldrich and used without further purification. Concentrations calculations were done with $x_{PW} = 7$ and $x_{SiW} = 25$. $C_3P_2$ was purchased from Sigma Aldrich and used as obtained. Milli-Q water was used with a conductivity lower than 10.5 µS/cm and a total organic carbon content of 400 ppb.

### *2.2 Cloud point (CP) measurements / pseudo-binary phase diagram*

For CP measurements, 3 g of ternary (water, $C_3P_2$ and POM/salt) mixtures were prepared into screwable tubes of borosilicate glass. The tubes were put into a thermostat (Thermomix_1460, B. Braun Melsungen AG) in special tube holders. The thermostat was heated with a heating rate of approximately 1 °C $min^{-1}$ and the phase separation was detected visually by the appearance of a white clouding in the sample. The expected precision of the measurements is approximately ± 1 °C.

### *2.3 Small angle X-ray scattering (SAXS)*

SAXS measurements, using Mo radiation ($\lambda$ = 0.071 nm), were performed on a bench built by XENOCS. The scattered beam was recorded using a large online scanner detector (diameter: 345 mm, from MAR Research). A large $q$-range (0.2 to 35 $nm^{-1}$) was covered with an off-center detection. The collimation was applied using a 12:$\propto$ multilayer Xenocs mirror (for Mo radiation) coupled to two sets of scatter less FORVIS slits providing a 0.8 × 0.8 mm X-ray beam at the sample position. Pre analysis of data was performed using the FIT2D software. The scattered intensities, *Intensity* or $I(q)$, are expressed versus the magnitude of scattering vector $q = [(4\pi)/\lambda]\sin(\theta/2)$, where $\lambda$ is the wavelength of incident radiation and $\theta$ the scattering angle. 2 mm quartz capillaries were used as sample containers for the solutions. Usual corrections for background (empty cell and detector noise) subtractions and intensity normalization using a high-density polyethylene film as a standard were applied. Experimental resolution was $\Delta Q/Q$ = 0.05. Silver behenate in a sealed capillary was used as the scattering vector calibration standard. All experiments were performed at 22 ± 2 °C.

### *2.4 Small angle neutron scattering (SANS)*

All measurements were performed on beamline D33 at the Institut Laue-Langevin (ILL) in Grenoble,

France. The measurements were made in time-of-flight (TOF) mode. All measurement parameters on D33 are controlled by the NOMAD software on site and were calibrated according to Dewhurst *et. al.*[26] Sample-to-detector distances were at 3 and 7 m with collimation at 7.8 m. This enables to cover an even larger $q$-range than using solely one detector at a fixed position. Afterwards both parts of the SANS spectra, detected by a set of 4+1 detectors, were merged and treated with the GRASP software on site. Note, that the merging of the spectra of the different panels make some inhomogeneities appear in the spectra at $q$ around 0.8 nm$^{-1}$. Water was used as a calibrant in order to obtain absolute intensities. Quartz cuvettes from Helma with thicknesses of 1 or 2 mm were used as sample containers. The samples were thermostated at 20 ± 1 °C. The acquisition times were set to 15 minutes taking into consideration sample thickness and composition, *i.e.* the level of scattering. Note, that the presented SANS spectra are subtracted by the signal of $D_2O$ but contain incoherent scattering due to the presence of H atoms in the samples.

## 3. Results and discussion

### *3.1 POMs in diluted $C_3P_2$ aqueous solutions*

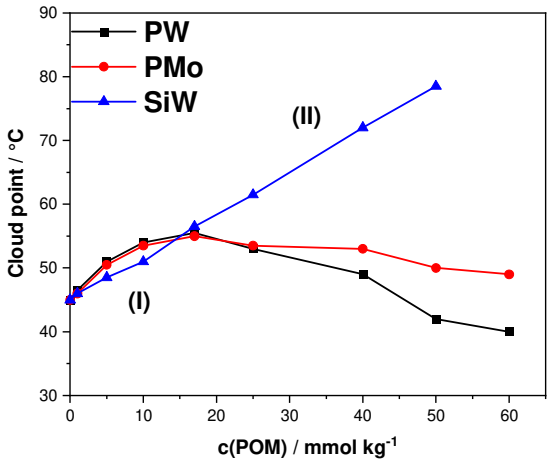


**Fig. 2.** Cloud point evolution of 10 wt% $C_3P_2$ in water as a function of POM concentration.

Fig. 2 shows the evolution of the CP of 10 wt% (0.57 mol kg$^{-1}$) $C_3P_2$ upon the addition of POMs: PW, SiW and phosphomolybdate (PMo). The CP of 10 wt% $C_3P_2$ is 45 °C which is in agreement with literature.[23][24] By adding POM, the CP evolution can be divided into two regimes: (I) with c(POM) ≤ 15 mmol kg$^{-1}$ and (II) with c(POM) > 15 mmol kg$^{-1}$. In regime (I) the CP is strongly increased, up to 55 °C, upon adding POMs. A high increase in the CP was previously observed for $C_8E_4$ and PNiPAM systems upon the addition of different POMs.[1][14] There it was shown by SAXS and SANS that this strong salting-in effect was due to the binding of POMs to $C_8E_4$ micelles and to the PNiPAM polymer chains. These native non-ionic systems become more hydrophilic upon binding with POMs because they acquire electrostatic repulsions from the bound, charged POMs. Therefore, the strong CP increase of $C_3P_2$ suggests that POMs interact with $C_3P_2$ in a comparable manner. In regime (I) the CP increase is more pronounced for PW and PMo compared to SiW. This trend, PW ~ PMo > SiW, was previously observed with the $C_8E_4$ micellar system and it was attributed to the lower charge density of PW/PMo (3-) compared to SiW (4-) which subsequently leads to a stronger binding.[2] This difference was therefore explained by a more favorable release of hydration water for PW/PMo compared to SiW, considering that the lower the charge density of the POM (or NI) the weaker their hydration. A stronger binding, *i.e.* a stronger SC behavior, for PW compared to SiW was also observed with cyclodextrin.[6] In regime (II) the CP is increased linearly upon further addition of SiW whereas the addition of PW and PMo cause a significant decrease of the CP. PW causes a more pronounced CP decrease, compared to PMo, even below the initial CP value of 45 °C. Hence, the increase in the POM concentration, in regime (II), produces a reversal of the series of the CP increase in regime (I): PW < PMo << SiW. Such a reversal in the SC behavior of POMs was, to the best of our knowledge, never reported in the literature so far.

In order to find an explanation for this unprecedented behavior, small angle X-ray and neutron scattering (SAXS and SANS) was performed on 10 wt% $C_3P_2$ solution with PW and SiW in regime (I) at 5 mmol kg$^{-1}$ and in regime (II) at 50 mmol kg$^{-1}$, see Fig. 3. For the SAXS, comparison was made with the SAXS spectra of POMs in pure water, as the scattering of POMs mainly contributes to the SAXS spectra. Indeed, the $C_3P_2$-water contrast is much weaker than the POM-water (or POM-$C_3P_2$) contrast. The spectra show the scattered intensity, $I(q)$ (provided in cm$^{-1}$), as a function of the wave vector, $q$ (given in nm$^{-1}$). For isotropic dispersions of finite size scattering objects, the scattered intensity may be expressed as: $I(q) = I(0)P(q)S(q)$ where $I(0)$ is the forward scattering, *cf.* Eq. S1. $P(q)$ and $S(q)$ are the form and structure factors which take into account respectively for the shape/size of the scattering objects and their interactions, which can be either repulsive or attractive depending on their size/shape/electrical charge and on the concentration of the scattering objects.

The SAXS spectra of SiW and PW in water in Fig. 3a/b show the typical scattering pattern of repulsive spherical (globular) scattering objects. The decrease in the scattered intensity visible for $q$ values above around 2 nm$^{-1}$ arises from the form factor, $P(q)$, of the Keggin POMs, which can be approximated as a sphere. The lower scattered intensity for $q$ < 2 nm$^{-1}$ arises from repulsive POM-POM interactions, $S(q)$, which is expected between electrically charged particles or scatterers in general. In case of 50 mmol kg$^{-1}$ of POMs, the overall scattered intensity is around ten times stronger than at 5 mmol kg$^{-1}$, which is expected according to Eq. S2. Moreover, broad peaks at intermediate $q$ values (see orange arrows in Fig. 3a/b) are clearly visible in the spectra at 50 mmol kg$^{-1}$ for PW and SiW, indicating stronger POM-POM repulsive interactions. These broad peaks are further described by Eq. S3. More detailed description and fits of the $P(q)$ and $S(q)$ of

POMs in water, which is out of scope here, have been the topic of previous contributions.[27][28][29]

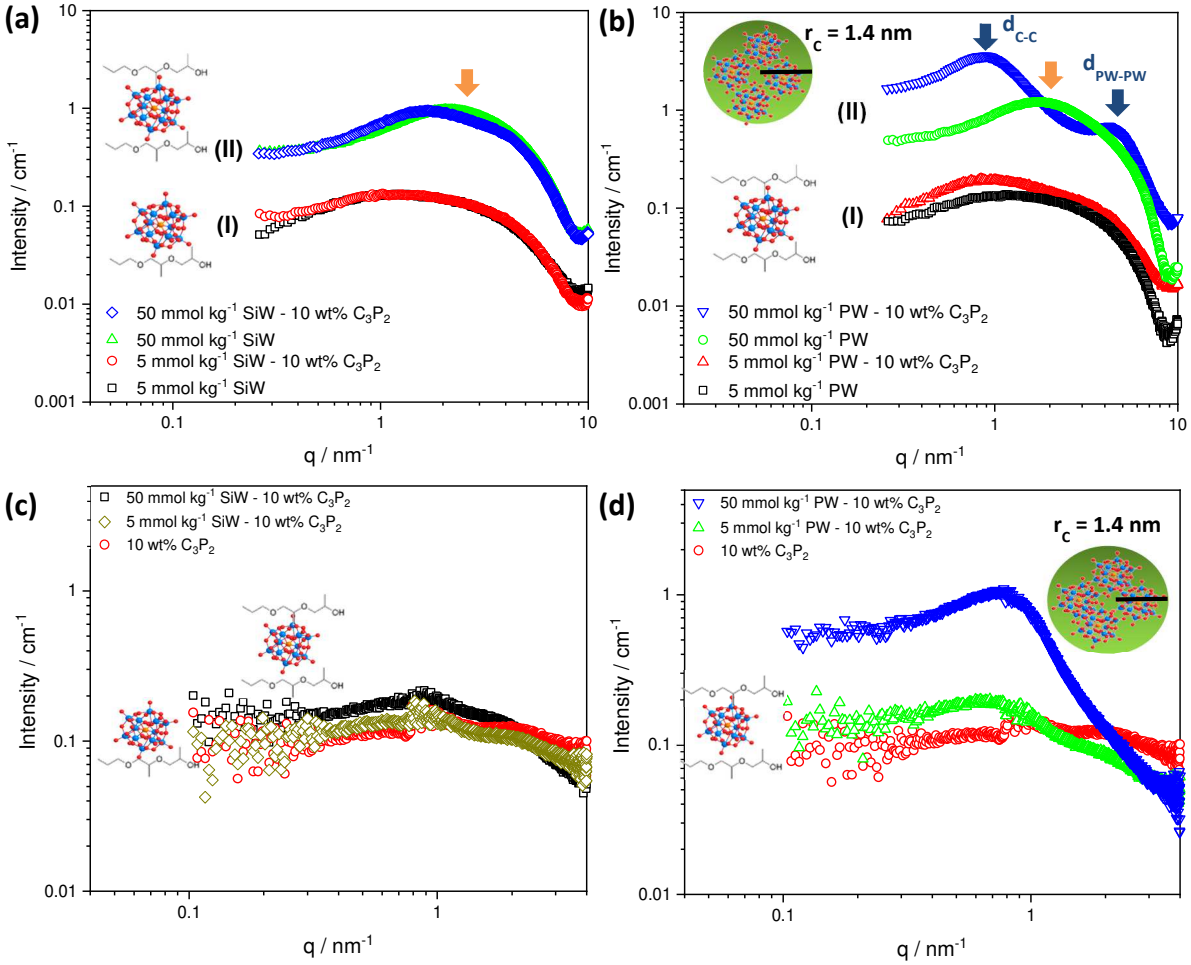


**Fig. 3.** SAXS spectra of (a) SiW in aqueous solution and in presence of 10 wt% $C_3P_2$ and (b) PW in aqueous solution and in presence of 10 wt% $C_3P_2$. (c) SANS spectra of SiW in 10 wt% $C_3P_2$ and (d) SANS spectra of PW in 10 wt% $C_3P_2$. $D_2O$ was used as solvent for the SANS measurements and the spectrum of 10 wt% $C_3P_2$ in $D_2O$ is given as a reference. All spectra are measured at room temperature, *i.e.* between 20 and 23 °C.

By changing the solvent from water to an aqueous solution containing 10 wt% $C_3P_2$ the spectrum of 5 mmol $kg^{-1}$ SiW shows nearly no evolution, whereas a slight modulation in the scattered intensity at intermediate $q$ range is observed for 50 mmol $kg^{-1}$, in comparison to the spectrum of 50 mmol $kg^{-1}$ SiW in pure water. This modulation induced by the presence of $C_3P_2$ may be attributed to the formation of nano-assemblies, such as SiW decorated with $C_3P_2$. The formation of SiW-$C_3P_2$ nano-assemblies, and therefore the binding of SiW and $C_3P_2$, implies a change in the local electron density around SiW due to a change in the solvation shell of the POM, *i.e.* the POM solvation water being partially substituted by $C_3P_2$. It has been shown in a previous investigation that POMs form such nano-assemblies with short chain PEGs and that the formation of such nano-assemblies produces a comparable modulation in the SAXS spectrum.[3] However, here the change in the SAXS spectrum induced by $C_3P_2$ is very weak which may be related either to (*i*) the weak contrast of $C_3P_2$ with the water compared to the POM-water (or POM-$C_3P_2$) contrast or to (*ii*) a too small number of $C_3P_2$ molecules in the close vicinity of the POMs (forming the nano-assemblies). To prove the (strong) interaction between SiW and $C_3P_2$, as deduced by the strong CP increase, $^1$H-NMR spectra of $C_3P_2$ (2 wt%) were recorded with an increasing concentration of SiW, see Fig. S1 and S2. Interestingly, upon the addition of SiW all signals of $C_3P_2$ are shifted, and some are partially splitted showing different multiplicities, which supports the hypothesis of strong SiW-$C_3P_2$ interactions, even though no change in the SAXS and SANS (see below) spectra were observed. A more detailed description of the $^1$H-NMR evolution is given in the supporting information.

For PW, the SAXS spectra are shown in Fig. 3b, for 5 and 50 mmol $kg^{-1}$ in water and in an aqueous solution containing 10 wt% $C_3P_2$. These two POM concentrations are compositions in regime (I) and in regime (II) respectively *cf.* Fig. 2. The SAXS spectrum of 5 mmol $kg^{-1}$ PW in presence of 10 wt% $C_3P_2$ shows a significant excess scattering, at $q < 2$ $nm^{-1}$, as previously observed for PW-PEG assemblies, *i.e.* PW decorated by in average two PEG oligomers.[3] Therefore, this excess scattering suggests PW-$C_3P_2$ nano-assemblies are formed. Indeed, the PW-$C_3P_2$ nano-assemblies are expected to produce excess scattering in the low $q$ range compared to bare PW because nano-assemblies are larger than the PW. Note, that for SiW at 5 mmol $kg^{-1}$ no excess scattering was

observed suggesting that no (or too few) SiW-$C_3P_2$ nano-assemblies are formed at low SiW concentration. In case of 50 mmol $kg^{-1}$ PW with 10 wt% $C_3P_2$ a much different scattering pattern is observed. Compared to the SAXS spectrum of 50 mmol $kg^{-1}$ PW in water (Fig. 3b green symbols), a several fold increase in the scattered intensity in the low $q$-range is observed in 10 wt% $C_3P_2$ medium (Fig. 3b blue symbols). Such a large scattering excess in the low $q$ range can only be explained by a clustering of several PWs. Indeed, the electron density of PW is very high compared to water or $C_3P_2$. Consequently, the scattering in SAXS is here nearly exclusively produced by the PW (or POM generally) and we can conclude that aggregates (or clusters) contain several PWs. Moreover, the excess scattering, due to these aggregates is observed in a $q$-range below 1.3 $nm^{-1}$, which informs on the size of the aggregates (3-5 nm). The SAXS spectrum also shows two strong correlation peaks at (*i*) $q_{max1}$ = 0.8 $nm^{-1}$ and (*ii*) $q_{max2}$ = 4 $nm^{-1}$. The peak at $q_{max1}$ = 0.8 $nm^{-1}$ can be attributed to cluster-cluster correlations. The decrease in the scattered intensity at $q$ < 0.8 $nm^{-1}$ is a signature of strong repulsive interactions, which are expected here as the clusters are constituted by several negatively charged POMs. According to Eq. S3, the average cluster-cluster distance is 7.9 nm. The correlation peak at $q_{max2}$ = 4 $nm^{-1}$ corresponds to correlations at much shorter distances and can be attributed to correlations between PWs in the clusters with a PW-PW distance of $d_{PW\text{-}PW}$ = 1.6 nm. Both the correlation peaks and the presence of electrostatic repulsions indicate the formation of colloidal particles (aggregates) formed by PW and presumably $C_3P_2$. It is remarkable, that the spectrum (blue symbols in Fig. 3b) shows an overall shape similar to the spectrum previously observed for a shell-decorated micelle consisting of a non-ionic surfactant and POMs in the micellar corona.[1][2] A fitting of this scattering curve is proposed in the following section.

In order to prove that the aggregates are constituted by $C_3P_2$ molecules, SANS was performed, see Fig. 3c/d, on samples with similar compositions as in Fig. 3a/b. However $D_2O$ was used instead of $H_2O$ to produce a good contrast between the hydrogenated $C_3P_2$ and all other contistutents ($D_2O$ and POM). The advantage of using SANS is that POMs (PW, SiW) have a very weak contrast with $D_2O$ whereas (hydrogenated) matter or molecules (here $C_3P_2$) produce good scattering due to the high H/D contrast. The scattering length density of the different compenents used here are listed later in Table 1. As a consequence, SANS is a complementary method to SAXS. SANS enables to investigate the clusterization of $C_3P_2$ molecules upon PW addition. The SANS spectrum of the aqueous 10 wt% $C_3P_2$ solution (red symbols in Fig. 3c/d) is almost flat, mainly due to incoherent scattering. It can be assumed that no significant aggregation occurs at 10 wt% $C_3P_2$, *i.e.* $C_3P_2$ molecules are well molecularly dispersed in $D_2O$ ($H_2O$). This result is in agreement with the negligible scattering measured in dynamic light scattering (DLS) suggesting that $C_3P_2$ molecules do not self-assemble, see Fig. S3.

Upon the addition of 5 mmol $kg^{-1}$ SiW the scattering curve remains unchanged. Hence, SANS does not show any larger nano-assemblies and supports the SAXS results (Fig. 3a red symbols). By increasing the concentration of SiW to 50 mmol $kg^{-1}$ (Fig. 3c dark symbols) the whole scattering curve is shifted by a factor of approximately two (from the red to the dark curve). This result suggests that around two $C_3P_2$ molecules self-assemble, presumably at the surface of a SiW anion. Moreover, a weak correlation peak is present at $q$ around 1 $nm^{-1}$, as observed in the SAXS spectrum (Fig. 3a blue symbols). As the correlation peaks are independent of the type of radiation used, it can be concluded that SAXS and SANS investigate the same scattering objects. Hence, the combination of SAXS and SANS indicates the formation of nano-assemblies, consisting of one SiW and approximately two $C_3P_2$ molecules, presumably replacing partially the SiW hydration water. Therefore, the combination of SANS, SAXS and $^1$H-NMR leads us to the conclusion, that 1:1 complexes between SiW and $C_3P_2$ complexes are formed at low concentrations of SiW (5 mmol $kg^{-1}$) and 1:2 complexes at high SiW concentrations (50 mmol $kg^{-1}$). This suggests sucessive formation of the complexes with the following equilibria, $C_3P_2$ (~ 0.57 mol $kg^{-1}$) being in these experiments always in large excess compared to SiW:

$$C_3P_2\,(\text{excess}) + \text{SiW} \leftrightarrow \text{SiW-}C_3P_2 \quad (1)$$

$$\text{SiW-}C_3P_2 + C_3P_2\,(\text{excess}) + \text{SiW} \leftrightarrow \text{SiW-}[C_3P_2]_2 \quad (2)$$

For PW, the SANS spectrum of 5 mmol $kg^{-1}$ PW in 10 wt% $C_3P_2$ (Fig. 3d) shows (*i*) an increase in the overall scattering by a factor of two (compared to the spectrum without PW, red symbols in Fig. 3d) and (*ii*) a correlation peak at $q$ = 0.8 $nm^{-1}$. This correlation peak again corresponds to the correlation peak observed by SAXS, see Fig. 3b red symbols. Consequently here for PW 5 mmol $kg^{-1}$, SAXS and SANS suggest the presence of PW-$C_3P_2$ (1:2) nano-assemblies, *i.e.* PW-$[C_3P_2]_2$. In case of 50 mmol $kg^{-1}$ PW in 10 wt% $C_3P_2$, the SANS spectrum shows, at $q$ < 1 $nm^{-1}$, a much stronger scattering, around eight to ten times stronger than the scattering obtained with 10 wt% $C_3P_2$. This is a clear signature of cluster formation containing several $C_3P_2$ molecules and with a size of around 3-5 nm. Moreover, a correlation peak is obtained at $q_{C\text{-}C}$ = 0.8 $nm^{-1}$, which is at the same position as the correlation peak observed in SAXS, $q_{max1}$ Fig. 3b, blue symbols. Therefore, here SAXS and SANS probes the same aggregates, which are consituted by several PW anions and $C_3P_2$ molecules. Moreover, in the low $q$-range, below 0.8 $nm^{-1}$, the scattered intensity decreases which indicates repulsive interactions between $[PW]_n[C_3P_2]_m$ aggregates, presumably of electrostatic origin as PW anions are likley to remain electrically charged in the aggregates.

As a conclusion here PW at low concentrations and SiW at high concentrations form nano-assemblies with one POM and two $C_3P_2$ molecules, whereas at high concentrations, PW shows a clear tendency to form colloidal size aggregates constituted by several PW and $C_3P_2$ molecules such as $[POM]_m[C_3P_2]_n$.

Therefore SiW and PW show a clear difference in their self-assembly behavior with $C_3P_2$, which can help to explain the different evolutions observed in the CP upon the addition of POM. Indeed two regimes (I) and (II) in the CP evolutions (Fig. 2) were distinguished and defined according to the different behavior of SiW and PW. In regime (I) the stronger increase in the CP obtained with PW (or PMo), compared to SiW, can be explained by a stronger binding constant with $C_3P_2$, as a result of a stronger superchaotropic character of PW compared to SiW. This assumption is further supported by SAXS and SANS as PW forms PW-$[C_3P_2]_2$ nano-assemblies at lower concentrations compared to SiW. In regime (II) at 50 mmol $kg^{-1}$, SiW still forms POM-$[C_3P_2]_2$ nano-assemblies, which is associated to a further increase of the CP, whereas PW leads to the formation of larger $[POM]_m[C_3P_2]_n$ aggregates which are less stable towards a temperature increase, *i.e.* leading to a decrease in the CP. It can be concluded here that the stronger superchaotropic behavior of PW, compared to SiW, promotes self-assembly, as a result of a stronger SC effect and/or weaker POM-POM electrostatic repulsions.

The stability of charged colloid dispersions is, in most cases, well understood in terms of the famous Derjaguin-Landau-Verwey-Overbeek (DLVO) theory[30] and is dominated by electrostatic repulsions and van der Waals attraction. More recent deviations from DLVO forces have been implemented by taking into account additional short-range repulsive "hydration" forces.[31][32] Here, the $[POM]_m[C_3P_2]_n$ colloids are charged and therefore stabilized by electrostatic repulsions, and most likely also by hydration forces. It is likely that the formation of $[POM]_m[C_3P_2]_n$ aggregates upon addition of PW reaches saturation, *i.e.* where a maximum amount of aggregate is formed. Indeed, CP evolution upon addition of (super)chaotropic salts have been previously fitted by a Langmuir adsorption isotherm model, which implies full coverage of surfaces by adsorbed species at high concentrations.[2][14][33] Further addition of PW, above the saturation limit, would therefore lead to unbound PW anions which can play the role of background salt and screen electrostatic repulsions between the $[POM]_m[C_3P_2]_n$ colloids. In previous contributions, the dual behavior of POMs, as background salts (3:1 or 4:1 salts) and as small charged colloids, has been discussed.[27] Therefore we propose here that the decrease in the CP in the regime (II) arises from the destabilization of the $[POM]_m[C_3P_2]_n$ colloids by screening of the electrostatic repulsions due to excess (unbound) PW. It can be assumed that hydration forces are not sufficient to keep the colloids stable, which is expected as the SC effect results from the favorable dehydration process of nano-ions and solutes (or surface or macrocycle).

*3.2 Investigation of* $[POM]_m$-$[C_3P_2]_n$ colloids

**Table 1.** Scattering length densities ($\rho$) of the different chemicals used in the study: PW, $C_3P_2$, $H_2O$ and $D_2O$ respectively for the SANS measurement.

| Compound | $\rho^{SANS}$ / $10^{-10}$ cm$^{-2}$ | $\rho^{SAXS}$ / $10^{-10}$ cm$^{-2}$ |
|---|---|---|
| PW | 5.92 | 86.9 |
| $H_2O$ | - | 9.47 |
| $D_2O$ | 6.33 | - |
| $C_3P_2$ | 0.08 | 8.65 |

This subsection contains further characterisations of the $[POM]_m[C_3P_2]_n$ colloids, noted here *c*, observed for 10 wt% $C_3P_2$ and 50 mmol $kg^{-1}$ of PW.

It is noteworthy, that the compound giving the major contrast in SAXS is the electron rich PW, whereas it is $C_3P_2$ in SANS, see the scattering length densities *($\rho$)* in Table 1. Therefore it can be assumed that $\rho^{SAXS}_{C_3P_2} \approx \rho^{SAXS}_{H_2O}$ *and* $\rho^{SANS}_{PW} \approx \rho^{SANS}_{D_2O}$. Hence, the scattering length densities of the colloids, *c*, can be expressed as:

$$\rho_C^{SAXS} = \\ = \Phi_C^{PW}\rho_{PW}^{SAXS} + \Phi_C^{H_2O}\rho_{H_2O}^{SAXS} + \Phi_C^{C_3P_2}\rho_{C_3P_2}^{SAXS} = \\ = \Phi_C^{PW}\rho_{PW}^{SAXS} + (1\text{-}\Phi_C^{PW})\,\rho_{H_2O}^{SAXS} \quad (3)$$

and

$$\rho_C^{SANS} = \\ = \Phi_C^{PW}\rho_{PW}^{SANS} + \Phi_C^{D_2O}\rho_{D_2O}^{SANS} + \Phi_C^{C_3P_2}\rho_{C_3P_2}^{SANS} = \\ = \Phi_C^{C_3P_2}\rho_{C_3P_2}^{SANS} + (1\text{-}\Phi_C^{C_3P_2})\,\rho_{D_2O}^{SANS} \quad (4)$$

where $\Phi_C^i$ and $\rho_i^{SAXS/SANS}$ are the volume fraction and the scattering length density of the component *i* (*i* = PW, $H_2O$ or $C_3P_2$) in the colloid *c*. The volume fraction of PW and $C_3P_2$ in the colloids can be expressed from Eq. (3) and (4) as

$$\Phi_C^{PW} = \frac{\rho_C^{SAXS} - \rho_{H_2O}^{SAXS}}{\rho_{PW}^{SAXS} - \rho_{H_2O}^{SAXS}} \quad (5)$$

$$\Phi_C^{C_3P_2} = \frac{\rho_C^{SANS} - \rho_{D_2O}^{SANS}}{\rho_{C_3P_2}^{SANS} - \rho_{D_2O}^{SANS}}. \quad (6)$$

The volume fraction of $H_2O$ (or $D_2O$) of the colloids is expressed as

$$\Phi_C^{H_2O} = 1\text{-}\Phi_C^{PW}\text{-}\Phi_C^{C_3P_2}. \quad (7)$$

The composition of the colloids, *i.e.* $\Phi_C^{H_2O}$, $\Phi_C^{PW}$ and $\Phi_C^{C_3P_2}$, can be determined from the scattering length density of the colloids: $\rho_C^{SANS}$ and $\rho_C^{SAXS}$. Numerical values of these scattering length densities can be obtained by fitting simultaneously the experimental SAXS/SANS in absolute scattering scale. For the fitting procedure, we considered a model of spheres, $P^{sphere}(q, r_C)$, with a homogenous scattering length density in the colloids, $\rho_C^{SANS}$ or $\rho_C^{SAXS}$ respectively for SANS and SAXS. A Hayter-MSA structure factor [34][35], $S^{HMSA}(q, R_{HS}, IS, \Phi_C, n_{charge})$, was used in order to take into account for the electrostatic repulsive interactions between the colloids. $IS$, $\Phi_C$, $n_{charge}$ are the ionic strength, the volume fraction of $c$ and the number of electrical charges per colloids. Note, that $\Phi_C$ is also contained and fitted in the prefactor, as $I(0) = n_c V_C^2 (\Delta\rho)^2 = \Phi_C V_C (\Delta\rho)^2$. This model was applied to the experimental SAXS and SANS spectrum, shown in Fig. 4. The experimental SAXS spectrum was subtracted by a constant of 0.55 cm$^{-1}$ to remove the POM contribution, in the range $q > 3$ nm$^{-1}$. Consequently, the focus here is made on the colloids, which mainly contributes to the scattering in the small angle part, $q < 3$ nm$^{-1}$. The simultaneous SAXS/SANS fit enables to perfectly reproduce the experimental spectra in absolute value, see Fig. 4. The numerical values of the fitting parameters, obtained for the best fit, are collected in Table 2. More details on the fitting procedure are given in the supporting information, Fig. S4 - S8 and Table S1 - S5.

**Table 2.** Numerical output values obtained for the simultaneous fitting of the SAXS and SANS spectra presented in Fig. 4. $r_C$, $\Phi_C$ and $n_{charge}$ are the colloids radius (from the form factor), the volume fraction and the number of charges of the colloid (from the structure factor). $\Phi_C$ was obtained from the prefactor $I(0)$.

| Fitting Parameters | value |
|---|---|
| $\rho_C^{SAXS}$ / 10$^{-10}$ cm$^{-2}$ | 19.89 |
| $\rho_C^{SANS}$ / 10$^{-10}$ cm$^{-2}$ | 1.11 |
| $r_C$ / nm | 1.40 |
| $\Phi_C$ | 0.02 |
| $n_{charge}(c)$ / e$^-$ | 10.9 |

The volume fractions of the three components in the colloids were calculated by using equations 5 and 6, see Table 3. Therefore, the values of the scattering length densities, $\rho_C^{SANS}$ and $\rho_C^{SAXS}$, obtained from the fit, *cf.* Table 2, were used. The number of PW, $C_3P_2$ and water molecules in a colloid ($N_C^i$) were consecutively calculated from the volume of the spherical colloids, $V_C = 4\pi r_C^3/3$, and $\Phi_C^i$ by

$$N_C^i = \frac{\Phi_C^i V_C}{V_i}. \qquad (8)$$

Here $V_i$ represents the molecular volume of the component $i$.

These results here enable to derive many representative conclusions on the formation of the colloids. They are mostly composed of $C_3P_2$ (84 vol%) and PW (14 vol%) and contain nearly no water, which goes in line with the driving force of the SC effect, *i.e.* the thermodynamically favourable dehydration of the nano-ion and the solute (or surface).

**Table 3.** Composition of the colloid $[PW]_m[C_3P_2]_n$ estimated by the simultaneous fit of the SAXS/SANS spectra. $\Phi_C^i$ and $N_C^i$ are the volume fractions and the numbers of $i$th components of the colloids.

| $i$ | $\Phi_C^i$ | $N_C^i$ |
|---|---|---|
| PW | 0.14 | 4.5 |
| $C_3P_2$ | 0.84 | 30.4 |
| $H_2O$ | 0.02 | 7.8 |

The total volume fraction of the colloids, $\Phi_C$, is around 2 vol% which is small compared to volume fraction of $C_3P_2$ (10 wt% ~ 9 vol%), indicating that a large quantity of $C_3P_2$ remains outside the colloids in surrounding solvent as monomers. The fraction of PW and $C_3P_2$ aggregated in the colloids can be further calculated:

$$c_{aggregated,\ i} = \frac{\Phi_C^i \Phi_C}{\Phi_{total}^i} \cdot c_{initial,\ i} \qquad (9)$$

This gives $c_{aggregated,\ PW}$ = 13 mmol kg$^{-1}$ and $c_{aggregated,\ C_3P_2}$ = 1.8 wt% = 102 mmol kg$^{-1}$, compared to the total concentrations 50 mmol kg$^{-1}$ of PW and 10 wt% $C_3P_2$, meaning that approximately 1/4 of the PW and 1/5 of $C_3P_2$ participates to the colloids. It is highly noteworthy, that $c_{aggregated,\ PW}$ = 13 mmol kg$^{-1}$ corresponds well with the boarder of regime (I) and (II) and supports the hypothesis of a saturation, where a maximum amount of colloids are formed as stated above. Therefore, the free or excess, PW can screen the electrostatic repulsions between the colloids promoting a decrease in the CP upon further increase in the PW concentrations as proposed

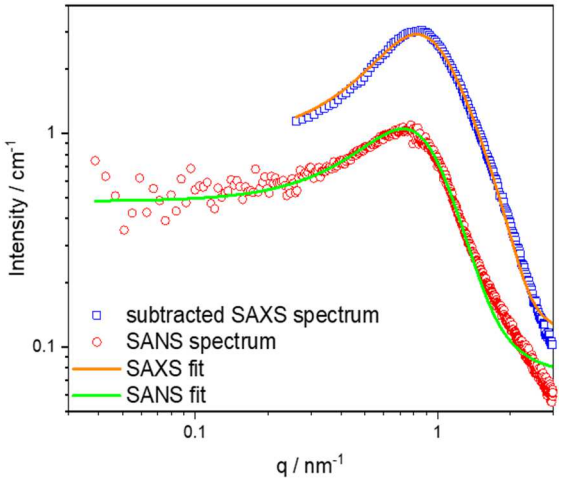


**Fig 4:** Subtracted SAXS spectrum and SANS spectrum of 10% $C_3P_2$ and 50 mmol kg$^{-1}$ of PW including a simultaneous fit (Hayter-MSA).

above by taking into account the DLVO theory.
Further quantitative information on the self-assembly of POMs are obtained by discussing the position of the correlation peaks in the SAXS spectra, informing on the average colloid-colloid distance, $d_{C-C} = \frac{2\pi}{q_{C-C}}$, see Fig. 3b. Indeed the average aggregation number of POM in the colloids, $N_C^{PW}$, can be estimated, by assuming a distribution of the colloids in a cubic lattice and from $d_{C-C}$ ,with the following equation:

$$d_{C-C} = \left(\frac{2\pi}{q^{C-C}}\right) = \sqrt[3]{\frac{N_C^{PW}}{c_{aggregated,\ PW} \cdot 6.02 \cdot 10^{-4}}} \qquad (10)$$

The peak position for 10 wt% $C_3P_2$ and 50 mmol $kg^{-1}$ is at $q_{C\text{-}C}$ = 0.85 $nm^{-1}$ which gives $N_C^{PW}$ = 3.2 if we consider $c_{aggregated,\ PW}$ = 13 mmol $kg^{-1}$. Note, that a detailed treatment of all peak positions in the measured SAXS spectra is given in Table S6. Moreover, we can calculate $N_C^{PW}$ from the number of charges of the colloids from the fitting results, *i.e.* 10.9. By assuming full dissociation of the counterion of PW, meaning that the effective charge of PW is 3-, then $N_C^{PW}$ = 10.9/3 = 3.6. Therefore, the three independent methods used here to estimate the number of PW in the colloids are in relatively good agreement, giving in average four PW in a colloid: $N_C^{PW}$ (from the fitting procedure) = 4.5, $N_C^{PW}$(from $q_{C\text{-}C}$) = 3.2 and $N_C^{PW}$(from $n_{charge}$) = 3.6. Moreover, this this validates the assumption that the counterions of the PW are mostly dissociated. Summarized, these treatments inform on the composition of $[POM]_m[C_3P_2]_n$ and lead us to the conclusion that m = 4 and n = 30, *i.e.* $[POM]_4[C_3P_2]_{30}$.

### *3.3 Effect of POMs on concentrated $C_3P_2$ solution*

In the following the effect of POMs is further investigated at high $C_3P_2$ content, x($C_3P_2$) = 55 wt% which is the composition at the LCST.[23] Fig. 5a shows the evolution of the CP upon the addition of POMs. The CP of 55 wt% $C_3P_2$ is at 14 °C, which is well in agreement with the LCST value in the literature.[23][24] PW, PMo and SiW also produce here a strong increase in the CP at low POM concentrations, up to around 25 mmol $kg^{-1}$. Upon further addition of POM two distinct behaviors appear:

*(i)* SiW produces a continuous increase of the CP, in a nearly linear fashion, up to 120 mmol $kg^{-1}$. For higher SiW concentrations, the CP keeps increasing up to above 100 °C.

*(ii)* PW/PMo produce a significantly less pronounced increase in the CP, reaching a maximum CP value of 29 and 30 °C respectively for PMo and PW at c(POM) = 100 mmol $kg^{-1}$. Then the CP decreases for higher POM concentrations.

The general trend of the CP evolution is comparable to the CP evolution of 10 wt% $C_3P_2$ upon addition of POMs, *cf.* Fig. 2. Nevertheless, the stronger SC of PW (or PMo) over SiW, which was obtained, at 10 wt% $C_3P_2$ and previously with many other systems[2][14], was not observed here at any POM concentrations. Note, that the CP evolution of 55 wt% $C_3P_2$ was investigated upon the addition of several additives, see Fig. S9 and Table S7. At low $C_3P_2$ concentrations (10 wt%) the origin for the lower CP of PW compared to SiW in regime (II) (see

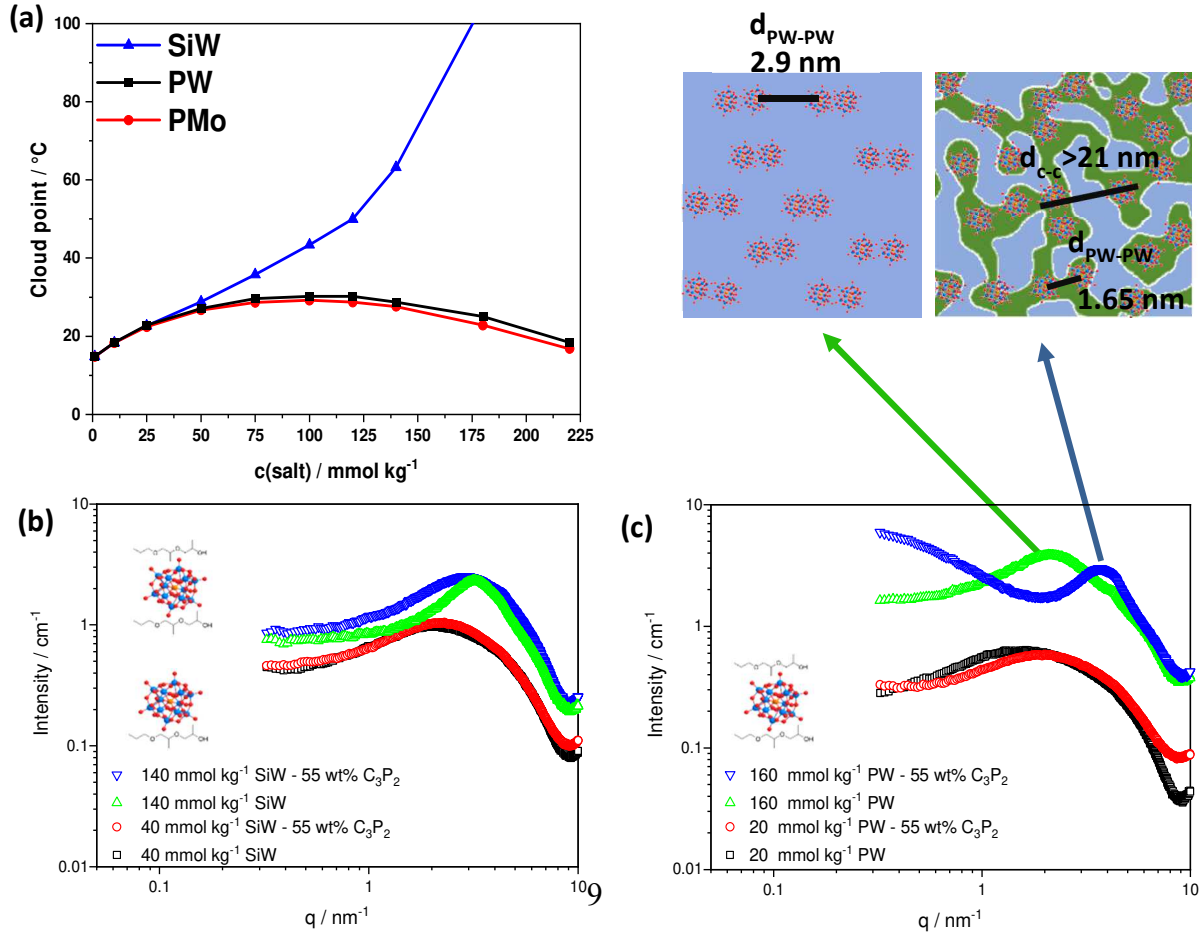


**Fig. 5.** (a) Cloud point evolution of 55 wt% $C_3P_2$ upon addition of POM. SAXS spectra, measured at room temperature, of (b) SiW in water and in 55 wt% $C_3P_2$ and (c) PW in water and in 55 wt% $C_3P_2$.

Fig. 2) was clearly attributed to the formation of $[POM]_m[C_3P_2]_n$ colloids, which is related to the stronger binding of PW with $C_3P_2$. Therefore, SAXS was performed here, in order to investigate if supramolecular assembly appears and if it can also help to explain the lower CP produced by PW compared to SiW.

Fig. 5b shows the SAXS spectra of 40 mmol $kg^{-1}$ and 140 mmol $kg^{-1}$ SiW in water and in 55 wt% $C_3P_2$. The SAXS spectrum of 40 mmol $kg^{-1}$ SiW in 55 wt% $C_3P_2$ shows nearly no difference with the SAXS spectrum of 40 mmol $kg^{-1}$ SiW in water. This indicates that $C_3P_2$ at such high concentrations does not produce assembly (colloids) of several SiW anions. Moreover, this suggests that, if there is a local change in the solvation sphere of SiW, this does not produce a noticeable difference in the SAXS pattern of the SiW, presumably due to a weak contrast between the solvation shell and the solvent (here $C_3P_2/H_2O$ 55 wt%/45 wt%). However, the strong CP increase suggests that strong interactions between SiW and $C_3P_2$ takes place in solution, as it was shown by $^1$H-NMR at lower $C_3P_2$ concentrations (2 wt%) above, see Fig. S2. For 140 mmol $kg^{-1}$ SiW in 55 wt% $C_3P_2$, the SAXS spectrum shows an intense peak, at $q$ = 3 $nm^{-1}$, which arises from the SiW-SiW structure factor and provides information on the average SiW-SiW distance (around $2\pi/q \approx$ 2.1 nm). This correlation peak is at the same position as in the SAXS spectrum of 140 mmol $kg^{-1}$ SiW in water but its shape is slightly different. Indeed, the peak is thinner in 55 wt% $C_3P_2$ than in water, which can be related to stronger SiW-SiW electrostatic repulsions, as expected from the lower permittivity of 55 wt% $C_3P_2$ compared to water. The presence of the peak in the SAXS spectrum arises from the first maximum in the structure factor and its position, at $q_{max}$, can be related here to the average POM-POM (or aggregate-aggregate) distance in solution, which corresponds to the first neighbor distance between scattering objects. This is only true if the form factor, $P(q)$, has a negligible effect on the peak position visible in the scattered intensity spectrum, $I(q)$, which results from the product (or convolution) of $P(q)$ and $S(q)$. The expected average SiW-SiW distance for a fully dispersed SiW solution, *i.e.* without SiW aggregation for a molecular solution, can be simply expressed from the SiW concentration, via Eq. (10) by considering a cubic arrangement of POM in solution. Therefore the $d_{SiW-SiW}$ at 140 mmol $kg^{-1}$ is expected to be around 2.3 nm which is close to the value obtained from the peak position in the SAXS spectrum, *i.e.* 2.1 nm, confirming that SiW is not aggregated in pure water nor in $C_3P_2$/water (55 wt%/45 wt%) mixture.

For PW 20 mmol $kg^{-1}$, the general scattering patterns of the PW at $q$ > 2 $nm^{-1}$, arising mainly from the PW form factor (sphere), are comparable in water and in 55 wt% $C_3P_2$. At lower $q$ values, a shift of the maximum in the scattered intensity is observed from 2 $nm^{-1}$ in pure water down to 1.2 $nm^{-1}$ in 55 wt% $C_3P_2$. The maximum in the scattered intensity can be related to the first order PW-PW correlation peak (structure factor), as discussed above. However, the peak is here too weak for further interpretation, in terms of the evaluation of the average PW-PW distance, as it is likely that its position may not be directly resulting from the first maximum in the structure factor. Indeed, a change in the solvent permittivity, water compared to $C_3P_2$/water (55 wt%/45 wt%), and a change in the local electron density of the PW, due to a different solvation, may affect respectively the structure factor (PW-PW) and the form factor of the solvated PW.

For 160 mmol $kg^{-1}$ PW, the SAXS spectrum shows a significantly different scattering pattern in water and in 55 wt% $C_3P_2$. In water, a distinct scattering peak is observed at 2.2 $nm^{-1}$, which corresponds to 2.9 nm in real space. If we assume monomers of PW, *i.e.* unaggregated form which are isotropically distributed in water, the PW-PW distance, $d_{PW-PW}$, is expected to be 2.2 nm (calculated from Eq. 10 with $N_C^{PW}$ = 1) and the peak position is expected at 2.9 $nm^{-1}$. This indicates that the correlation peak corresponds to correlation between aggregates, and not between PW anions. Therefore, PW at 160 mmol $kg^{-1}$ is already aggregated in water with an average aggregation number ($N_c^{POM}$) of 2.2, as calculated from the peak position, at 2.2 $nm^{-1}$ ($d_{PW-PW}$ = 2.9 nm) from Eq. 10.

This result is in good agreement with the previous work of Bera *et. al.* that has shown, by synchrotron SAXS experiments at high $q$ range and by molecular dynamics (MD) simulation, the general tendency of PW to self-assemble in water at high concentrations.[28] Indeed, these authors have shown that PW form aggregates constituted of several PW anions (dimers, trimers, etc.) and that these aggregates turn into larger percolating structures by increasing PW concentration. The presence of these large scattering objects was also detected by using DLS.[27] Therefore, it appears here that PW at 160 mmol $kg^{-1}$ is mostly present as dimers in water, as sketched in Fig. 5c (left sketch).

The spectrum for PW at 160 mmol $kg^{-1}$ is very much different in 55 wt% $C_3P_2$, compared to the spectrum in pure water, as it shows a correlation peak at higher $q$ values and a large scattering excess at low $q$. The peak at higher $q$ is observed at 3.8 $nm^{-1}$, which corresponds to 1.65 nm in real space. Considering that the PW dimension is around 1 nm, this latter peak can be attributed to an internal structure factor, *i.e.* to PW-PW correlations inside the aggregates. Indeed, the presence of POM aggregates is confirmed in the low q-regime, for $q$ < 2 $nm^{-1}$, where a strong excess scattering is observed. Therefore, PW self-aggregates in mesoscopic structures in $C_3P_2$ 55 wt%. The size of these aggregates is larger than 21 nm *cf.* Eq. S4. It can be noted that the PW-PW distance in the aggregate (1.65 nm) is larger than the expected PW-PW distance at close contact, which is around the size of PW, ~ 1 nm. Therefore, it is likely that the aggregates contain $C_3P_2$ molecules between the PWs. To investigate these objects further, SAXS measurements should be performed at lower angles in order to find out if the aggregates have a finite size, as in the case of the composition 10 wt% $C_3P_2$ and 50 mmol $kg^{-1}$ of PW. Note, that several more SAXS measurements at different POM concentrations in water and in 55 wt% $C_3P_2$ are shown in Fig. S10 and S11.

Nevertheless, here no aggregate-aggregate peak is visible in the spectrum, probably because it appears

at $q$ lower than 0.3 nm$^{-1}$. Consequently, we can conclude that the PW aggregation number is larger than 885 (calculated from a peak position of 0.3 nm$^{-1}$ from Eq. 10). This result suggests that the PW aggregates have no finite size, such as encountered in microemulsions with a bicontinuous structure or with an interconnected cylinder network or surfactant free-microemulsion. This hypothesis is further supported by the large concentrations of the three components: water, $C_3P_2$ and PW, which favours such interconnected structures. If we assume that such infinite size structures form, two pseudo phases should be present: a water-rich and a $C_3P_2$-rich phase, *i.e.* the PW aggregated phase or the pseudo-phase where PW accumulates. A sketch representing a hypothetical bicontinuous-like mesoscale structure is given as an example in Fig. 5c (right). PW is likely to accumulate in the $C_3P_2$ pseudo-phase, as it was shown by NMR that POMs and $C_3P_2$ strongly interact and obtained in Fig. S12. In such a case, the peak position, at 3.8 nm$^{-1}$, informs on the PW concentration in the $C_3P_2$ rich pseudo phase. By considering evenly distributed PW in a cubic pattern, with $d_{PW\text{-}PW}$ = 1.65 nm, the PW concentration in the $C_3P_2$ phase can be roughly estimated by using Eq. 10, by taking $N_C^{PW}$ = 1, which gives 357 mmol kg$^{-1}$. This concentration is then around two times larger than the bulk PW concentration in the whole sample (160 mmol kg$^{-1}$). This is well in agreement with our hypothesis of the formation of two pseudo phases, where PW accumulates in the $C_3P_2$ pseudo phase. Indeed $C_3P_2$ in the $C_3P_2$/water mixture is around 55 wt%, therefore the concentration of PW accumulated in a $C_3P_2$ pseudo phase, which is probed by the PW-PW peak position observed in SAXS, is expected to be around two times larger than the total bulk PW concentration.

As a conclusion here, the decrease in the CP observed with PW at high concentration (> 100 mmol kg$^{-1}$, see Fig. 5a), is concomitant with the appearance of mesoscale structuration (aggregation of many PW with $C_3P_2$). This is comparable to the conclusion made at lower $C_3P_2$ content in water (at 10 wt%), that has also shown that the appearance of aggregates, *i.e.* in this case $[POM]_m[C_3P_2]_n$ colloids with m~4 and n~30, led to the decrease in the CP. On the contrary, SiW does not self-aggregate in small colloids or mesoscale structures, and lead to a continuous increase in the CP upon POM addition. This different tendency for self-assembly between PW/PMo and SiW seems to be related to the properties of these POMs in water. Indeed, the tendency of PW to self-assemble, compared to SiW, was already observed in pure water.[27][28]

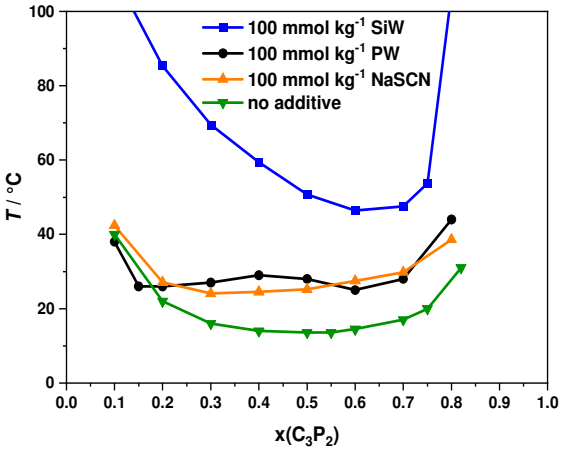


**Fig. 6.** Influence of PW, SiW and NaSCN on the binary phase diagram water-$C_3P_2$. The lines represent the liquid-liquid phase demixion line. Above these lines the system phase separates into two macroscopic liquid phases, one water-rich and one $C_3P_2$ rich-phase.

In the following, the effect of POM is investigated over a large range of $C_3P_2$/water ratios in order to give an overview of the SC effect of Keggin's POMs on the evolution of the phase diagram of this short chain amphiphilic molecule in water. Fig. 6 shows the binary water-$C_3P_2$ phase diagram and the influence of a constant concentration of c = 100 mmol kg$^{-1}$ SiW, PW and NaSCN, which can be considered as a classical chaotropic ion. As previously stated, the system water-$C_3P_2$ shows a LCST, 14 °C, at x($C_3P_2$) = 55 wt%, see the green curve in Fig. 6. Upon the addition of NaSCN, *i.e.* 100 mmol kg$^{-1}$, the biphasic region is shifted to higher temperatures. The LCST increases by 10 °C, up to 24 °C. This fact arises due to the salting-in ability of the chaotropic $SCN^-$ and was already intensively investigated.[24][25] Upon the addition of 100 mmol kg$^{-1}$ SiW the phase boundary is shifted to even higher temperatures, *i.e.* the LCST is raised to 46 °C. This is caused by the strong interaction of the superchaotropic SiW with $C_3P_2$. The influence of PW in contrast causes both: (*i*) an increase of the co-miscibility of water-$C_3P_2$ (x($C_3P_2$) > 0.2) and also (*ii*) a decrease of the co-miscibility (x($C_3P_2$) < 0.2). On the one hand, the increase in co-miscibility for (x($C_3P_2$) > 0.2) can be explained by the general ability of PW to interact strongly with $C_3P_2$. On the other hand, the decrease in solubility for (x($C_3P_2$) < 0.2) can be explained by the formation of $C_3P_2$/PW co-assemblies, which promotes a macroscopic liquid-liquid phase separation upon temperature increase.

It is remarkable, that the interaction of common proteins (*e.g.* human serum albumin (HSA)) with surfaces (either charged or uncharged) is not only dictated by electrostatic interactions.[36][37] For example, the protein adsorption on uncharged surfaces such as polytetrafluorethylene (PTFE) was described by a sum of various components, *e.g.* dispersion forces and Lifshitz-van der Waals forces.[38] POMs also interact via a combination of diverse intermolecular forces, electrostostatic, hydration forces, hydrophobic effect and dispersion forces. Therefore, POMs are, in that sense, comparable to proteins. As POMs are known to be catalytically active[39] they may be called artificial enzymes or nanozyme, as already investigated by several research groups.[40][41][42]

## 4. Conclusion

In this contribution, we show that the Keggin-type POMs, SiW and PW/PMo, interact strongly in water with a short chain non-ionic amphiphile, $C_3P_2$, that is too short to form micelles in water compared to classical surfactants. The strong POM-$C_3P_2$ interaction (or binding) results from the thermodynamically favorable dehydration of POM and $C_3P_2$, *i.e.* the superchaotropic effect. This effect was observed here through the significant increase in the CP of $C_3P_2$ and by NMR measurements. At low POM concentrations (below 15 mmol kg$^{-1}$) and

at 10 wt% $C_3P_2$, a stronger superchaotropic behavior was observed for PW (and PMo) over SiW, resulting from the lower charge density for PW(3-) over SiW(4-). Lower charge density nano-ions have a weaker hydration and, therefore, their dehydration is easier (or more favorable). This trend in the superchaotropicity of Keggin's POMs, PW ~ PMo > SiW, was observed previously with many other systems: non-ionic surfactants (polyethoxylated and glucose based)[1][2], PEG oligomers[3], PNiPAM[14], lipids monolayer[43], γ-CD[4].

At higher POM concentrations (above 15 mmol $kg^{-1}$), SiW shows a continuous increase in the CP as a result of strong SiW-$C_3P_2$ attractive interactions. The combination of SAXS/SANS/NMR shows that SiW forms small nano-assemblies, such as $[SiW][C_3P_2]_{1-2}$. On the contrary, PW leads to a decrease in the CP which is concomitant with the formation of larger aggregates: (*i*) containing many PW anions and $C_3P_2$, with the general formula $[PW]_n[C_3P_2]_m$ at 10 wt% $C_3P_2$ , with n~4 and m~30, and (*ii*) percolated (interconnected, bicontinuous-like) structures at 55 wt% $C_3P_2$. This latter structure shows the thermodynamically stable coexistence of two pseudo phases: a water-rich phase and a $C_3P_2$-rich phase where PW accumulates (*i.e.* the percolated-like structure). In this $C_3P_2$-rich phase, the average PW-PW distance is around 1.65 nm and the size domain of this structure is above 21 nm.

It seems that the formation of PW aggregates, *i.e.* $[PW]_n[C_3P_2]_m$ and interconnected structure, is related to the intrinsic tendency of PW (or PMo) to self-assemble in water, as shown previously by Bera *et. al.*[28] On the contrary, SiW does not form self-assembly colloids containing many SiW anions in water, presumably because of too strong SiW-SiW electrostatic repulsions preventing their self-assembly. However, SiW interacts strongly with $C_3P_2$, as inferred by the continuous increase in the CP upon increasing SiW concentration, whereas PW only leads to an increase in the CP at low concentrations, *i.e.* where it does not self-assemble. The decrease in the CP by further increasing PW concentration is proposed to be due to the screening of the electrostatic repulsions between the $[PW]_n[C_3P_2]_m$, by the excess PW increasing the ionic strength. This screening effect leads to the destabilization of the $[PW]_n[C_3P_2]_m$ colloids and to the phase demixion, and consequently to the decrease in the CP. This process is comparable to the destabilization mechanism of charge colloidal suspensions that is well understood by the DLVO theory.

As a conclusion, we show here for the first time that:

*(i)* PW induces the self-assembly of a short amphiphilic molecule with hydrophobic character, here a polypropylene glycol alkyl ether, in water, and that

*(ii)* SiW, at high concentrations, has a stronger salting-in property, *i.e.* a stronger increase in the CP of $C_3P_2$, compared to PW, because of the formation of $[PW]_n[C_3P_2]_m$ colloids.

This stronger salting-in effect of SiW over PW results therefore in a drastic enhancement of the co-miscibility of $C_3P_2$ and water, up to reaching full co-miscibility at room temperature, see the phase diagram in Fig. 6. Considering that POMs are photo-catalytically active, the present results open new opportunities in the design of (water-organic) solvent media with controlled nano-structures to perform photochemical reactions.

## 5. Acknowledgements

We are grateful to the CNRS for the international Research Project Nano-Ions at Soft Interfaces, Max Hohenschutz for fruitful discussion, Bruno Corso, Xavier Legoff for technical support with the SAXS apparatus and Isabelle Grillo for assistance with the SANS measurements.

## 6. Bibliography

[1] B. Naskar, O. Diat, V. Nardello-Rataj, P. Bauduin, Nanometer-Size Polyoxometalate Anions Adsorb Strongly on Neutral Soft Surfaces, J. Phys. Chem. C. 119 (2015) 20985–20992. https://doi.org/10.1021/acs.jpcc.5b06273.

[2] T. Buchecker, P. Schmid, S. Renaudineau, O. Diat, A. Proust, A. Pfitzner, P. Bauduin, Polyoxometalates in the Hofmeister series, Chem. Commun. 54 (2018) 1833–1836. https://doi.org/10.1039/c7cc09113c.

[3] T. Buchecker, X. LeGoff, B. Naskar, A. Pfitzner, O. Diat, P. Bauduin, Polyoxometalate / polyethylene glycol interactions in water : From nano-assemblies in water to crystal formation by electrostatic screening, Chem. - A Eur. J. 23 (2017) 8434–8442. https://doi.org/10.1002/chem.201700044.

[4] K.I. Assaf, M.S. Ural, F. Pan, T. Georgiev, S. Simova, K. Rissanen, D. Gabel, W.M. Nau, Water structure recovery in chaotropic anion recognition: High-affinity binding of dodecaborate clusters to γ-cyclodextrin, Angew. Chemie - Int. Ed. 54 (2015) 6852–6856. https://doi.org/10.1002/anie.201412485.

[5] S. Yao, C. Falaise, A.A. Ivanov, N. Leclerc, M. Hohenschutz, M. Haouas, D. Landy, M.A. Shestopalov, P. Bauduin, E. Cadot, Hofmeister effect in the Keggin-type polyoxotungstate series, Inorg. Chem. Front. (2020). https://doi.org/10.1039/D0QI00902D.

[6] K.I. Assaf, W.M. Nau, The Chaotropic Effect as an Assembly Motif in Chemistry, Angew. Chemie - Int. Ed. 57 (2018) 13968–13981. https://doi.org/10.1002/anie.201804597.

[7] W. Kunz, Specific ion effects, World Scientific, 2010. https://doi.org/https://doi.org/10.1142/7261.

[8] W. Kunz, J. Henle, B.W. Ninham, "Zur Lehre von der Wirkung der Salze" (about the science of the effect of salts): Franz Hofmeister's historical papers, Curr. Opin. Colloid Interface Sci. 9 (2004) 19–37. https://doi.org/10.1016/j.cocis.2004.05.005.

[9] L. Pérez-Fuentes, D. Bastos-González, J. Faraudo, C. Drummond, Effect of organic and inorganic ions on the lower critical solution transition and aggregation of

PNIPAM, Soft Matter. 14 (2018) 7818–7828. https://doi.org/10.1039/c8sm01679h.
[10] M. Christoforou, E. Leontidis, G. Brezesinski, Effects of sodium salts of lyotropic anions on low-temperature, ordered lipid monolayers, J. Phys. Chem. B. 116 (2012) 14602–14612. https://doi.org/10.1021/jp307004e.
[11] M. Hohenschutz, I. Grillo, O. Diat, P. Bauduin, How Nano-Ions Act Like Ionic Surfactants, Angew. Chemie - Int. Ed. 59 (2020) 8084–8088. https://doi.org/10.1002/anie.201916193.
[12] P. Bauduin, S. Prevost, P. Farràs, F. Teixidor, O. Diat, T. Zemb, A theta-shaped amphiphilic cobaltabisdicarbollide anion: Transition from monolayer vesicles to micelles, Angew. Chemie - Int. Ed. 50 (2011) 5298–5300. https://doi.org/10.1002/anie.201100410.
[13] C. Drummond, L. Pérez-Fuentes, D. Bastos-González, Can Polyoxometalates be Considered as Super-Chaotropic Ions?, J. Phys. Chem. C. 123 (2019) 28744–28752. https://doi.org/https://doi.org/10.1021/acs.jpcc.9b08324.
[14] T. Buchecker, P. Schmid, I. Grillo, S. Prévost, M. Drechsler, O. Diat, A. Pfitzner, P. Bauduin, Self-assembly of short chain Poly-N-isopropylacrylamid (PNIPAM) induced by superchaotropic Keggin Polyoxometalates: from globules to sheets., J. Am. Chem. Soc. 141 (2019) 6890–6899. https://doi.org/10.1021/jacs.8b12181.
[15] A. Misra, K. Kozma, C. Streb, M. Nyman, Beyond Charge Balance: Counter-Cations in Polyoxometalate Chemistry, Angew. Chemie - Int. Ed. 59 (2019) 596–612. https://doi.org/10.1002/anie.201905600.
[16] C. Falaise, M.A. Moussawi, S. Floquet, P.A. Abramov, M.N. Sokolov, M. Haouas, E. Cadot, Probing Dynamic Library of Metal-Oxo Building Blocks with γ-Cyclodextrin, J. Am. Chem. Soc. 140 (2018) 11198–11201. https://doi.org/10.1021/jacs.8b07525.
[17] D. Stoye, Solvents, in: Ulmann`s Encycl. Ind. Chemsitry, Wiley-VCH Verlag GmbH & Co. KGaA, Weinheim, 2012: pp. 619–688. https://doi.org/10.1002/14356007.a24.
[18] W. Kunz, K. Holmberg, T. Zemb, Hydrotropes, Curr. Opin. Colloid Interface Sci. 22 (2016) 99–107. https://doi.org/10.1016/j.cocis.2016.03.005.
[19] S.E. Friberg, Hydrotropes, Curr. Opin. Colloid Interface Sci. 2 (1997) 490–494. https://doi.org/10.1016/S1359-0294(97)80096-9.
[20] T.K. Hodgdon, E.W. Kaler, Hydrotropic solutions, Curr. Opin. Colloid Interface Sci. 12 (2007) 121–128. https://doi.org/10.1016/j.cocis.2007.06.004.
[21] D. Evans, H. Wennerström, The Colloidal Domain, Second edi, Wiley, 1999.
[22] T. Buchecker, S. Krickl, R. Winkler, I. Grillo, P. Bauduin, D. Touraud, A. Pfitzner, W. Kunz, The impact of the structuring of hydrotropes in water on the mesoscale solubilisation of a third hydrophobic component, Phys. Chem. Chem. Phys. 19 (2017) 1806–1816. https://doi.org/10.1039/c6cp06696h.
[23] P. Bauduin, L. Wattebled, S. Schrödle, D. Touraud, W. Kunz, Temperature dependence of industrial propylene glycol alkyl ether/water mixtures, J. Mol. Liq. 115 (2004) 23–28. https://doi.org/10.1016/j.molliq.2004.01.001.
[24] G. Grundl, M. Müller, D. Touraud, W. Kunz, Salting-out and salting-in effects of organic compounds and applications of the salting-out effect of Pentasodium phytate in different extraction processes, J. Mol. Liq. 236 (2017) 368–375. https://doi.org/10.1016/j.molliq.2017.03.091.
[25] P. Bauduin, L. Wattebled, D. Touraud, W. Kunz, Hofmeister ion effects on the phase diagrams of water-propylene glycol propyl ethers, Zeitschrift Fur Phys. Chemie. 218 (2004) 631–641. https://doi.org/10.1524/zpch.218.6.631.33453.
[26] C.D. Dewhurst, I. Grillo, D. Honecker, M. Bonnaud, M. Jacques, C. Amrouni, A. Perillo-Marcone, G. Manzin, R. Cubitt, The small-angle neutron scattering instrument D33 at the Institut Laue – Langevin, J. Appl. Crystallogr. 49 (2016) 1–14. https://doi.org/10.1107/S1600576715021792.
[27] A. Malinenko, A. Jonchère, L. Girard, S. Parrès-Maynadié, O. Diat, P. Bauduin, Are Keggin's POMs Charged Nanocolloids or Multicharged Anions?, Langmuir. 34 (2018) 2026–2038. https://doi.org/10.1021/acs.langmuir.7b03640.
[28] M.K. Bera, B. Qiao, S. Seifert, B.P. Burton-Pye, M. Olvera De La Cruz, M.R. Antonio, Aggregation of Heteropolyanions in Aqueous Solutions Exhibiting Short-Range Attractions and Long-Range Repulsions, J. Phys. Chem. C. 120 (2016) 1317–1327. https://doi.org/10.1021/acs.jpcc.5b10609.
[29] M.R. Antonio, M.K. Bera, pH-Dependent Interactions between Keggin Heteropolyanions in Dilute Solutions, Eur. J. Inorg. Chem. 2019 (2019) 367–373. https://doi.org/10.1002/ejic.201801165.
[30] J. Isrealachvili, Intermolecular and Surface Forces, 3rd ed., Academic Press, London, 2013.
[31] J.A. Molina-Bolívar, F. Galisteo-González, R. Hidalgo-Alvarez, The role played by hydration forces in the stability of protein-coated particles: Non-classical DLVO behaviour, Colloids Surfaces B Biointerfaces. 14 (1999) 3–17. https://doi.org/10.1016/S0927-7765(99)00020-X.
[32] R.M. Pashley, DLVO and hydration forces between mica surfaces in Li+, Na+, K+, and Cs+ electrolyte solutions: A correlation of double-layer and hydration forces with surface cation exchange properties, J. Colloid Interface Sci. 83 (1981) 531–546. https://doi.org/10.1016/0021-

9797(81)90348-9.
[33] Y. Zhang, S. Furyk, D.E. Bergbreiter, P.S. Cremer, Specific ion effects on the water solubility of macromolecules: PNIPAM and the Hofmeister series, J. Am. Chem. Soc. 127 (2005) 14505–14510. https://doi.org/10.1021/ja0546424.
[34] P. Taylor, J.B. Hayter, J. Penfold, Molecular Physics : An International Journal at the Interface Between Chemistry and Physics An analytic structure factor for macroion solutions, Mol. Phys. 42 (1981) 109–118. https://doi.org/10.1080/00268978100100091.
[35] J. Hansen, J.B. Hayter, A rescaled MSA structure factor for dilute charged colloidal dispersions, Mol. Phys. An Int. J. Interface Between Chem. Phys. 43 (2006) 651–656. https://doi.org/http://dx.doi.org/10.1080/00268978200101471.
[36] C.M. Roth, A.M. Lenhoff, Electrostatic and van der Waals Contributions to Protein Adsorption: Computation of Equilibrium Constants, Langmuir. 9 (1993) 962–972. https://doi.org/10.1021/la00028a015.
[37] W. Norde, Driving forces for protein adsorption at solid surfaces, Macromol. Symp. 103 (1996) 5–18. https://doi.org/10.1002/masy.19961030104.
[38] C.J. Van Oss, R.J. Good, M.K. Chaudhury, The role of van der Waals forces and hydrogen bonds in “hydrophobic interactions” between biopolymers and low energy surfaces, J. Colloid Interface Sci. 111 (1986) 378–390. https://doi.org/10.1016/0021-9797(86)90041-X.
[39] S. Krickl, T. Buchecker, A.U. Meyer, I. Grillo, D. Touraud, P. Bauduin, B. König, A. Pfitzner, W. Kunz, A systematic study of the influence of mesoscale structuring on the kinetics of a chemical reaction, Phys. Chem. Chem. Phys. 19 (2017) 23773–23780. https://doi.org/10.1039/C7CP02134H.
[40] B. Zhang, M. Zhao, Y. Qi, R. Tian, B.B. Carter, H. Zou, C. Zhang, C. Wang, The Intrinsic Enzyme Activities of the Classic Polyoxometalates, Sci. Rep. 9 (2019) 1–12. https://doi.org/10.1038/s41598-019-50539-9.
[41] Y. He, X. Li, X. Xu, J. Pan, X. Niu, A cobalt-based polyoxometalate nanozyme with high peroxidase-mimicking activity at neutral pH for one-pot colorimetric analysis of glucose, J. Mater. Chem. B. 6 (2018) 5750–5755. https://doi.org/10.1039/c8tb01853g.
[42] N. Gao, K. Dong, A. Zhao, H. Sun, Y. Wang, J. Ren, X. Qu, Polyoxometalate-based nanozyme: Design of a multifunctional enzyme for multi-faceted treatment of Alzheimer’s disease, Nano Res. 9 (2016) 1079–1090. https://doi.org/10.1007/s12274-016-1000-6.
[43] D. Kobayashi, H. Nakahara, O. Shibata, K. Unoura, H. Nabika, Interplay of Hydrophobic and Electrostatic Interactions between Polyoxometalates and Lipid Molecules, (2017). https://doi.org/10.1021/acs.jpcc.7b01774.